Astron. Astrophys. 321, 311–322 (1997)

ASTRONOMY AND ASTROPHYSICS

Determination of molecular cloud parameters using thermal methanol lines

S.V. Kalenskii[1], **A.M. Dzura**[1], **R.S. Booth**[2], **A. Winnberg**[2], **and A.V. Alakoz**[3]

[1] Astro Space Center of Lebedev Physical Institute, Profsoyuznaya 84/32, 117810 Moscow, Russia
[2] Onsala Space Observatory, S-439 92 Onsala, Sweden
[3] Moscow State University, Physical Faculty, Astronomical Department, Universitetskii pr. 13, 119899 Moscow, Russia

Received 16 February 1996 / Accepted 17 September 1996

Abstract. The $2_K - 1_K$ thermal methanol lines near 96 GHz were detected toward 12 regions of massive star formation. Together with the $J_0 - J_{-1}E$ lines observed previously, they were used to determine temperature, density, methanol abundance, and some other parameters of interest. Two methods were used to determine the same set of parameters: a simplified analytical method and statistical equilibrium calculations; the results are in satisfactory agreement with each other. The source kinetic temperatures are in the range 15-50 K, densities in the range 0.3-5 $\times 10^6$ cm^{-3}, and methanol abundance in the range $4 \times 10^{-10} - 1.7 \times 10^{-7}$. Broad wings indicating high-velocity motions were detected toward a number of sources.

Key words: ISM: clouds – ISM: molecules – ISM: abundances radio lines: ISM

1. Introduction

Regions of massive star formation have been extensively studied in the lines of simple molecules like CO, CS, or NH_3. In contrast, only a few have been carefully studied in thermal lines of more complex molecules, such as methanol (CH_3OH) or methyl cyanide (CH_3CN). Complex molecules are less abundant than simpler ones and their thermal lines are typically weak, making observations of them difficult. However, observations of these molecules are very important for interstellar chemistry; in addition, the richness of their spectra and tendency to form groups of lines, which can be observed simultaneously with the same telescope and receiver, allows one to obtain information about physical parameters of the sources which sometimes cannot be obtained from observations of simple molecules.

Methanol is one of the most abundant complex molecules in Galactic star-forming regions. The methanol molecule is a slightly asymmetric top with hindered internal rotation, and possesses a large number of allowed transitions at radio frequencies. Methanol in space has been intensively studied since its discovery by Ball et al. (1970), but the attention has mostly been concentrated on methanol masers, and much less effort has been spent on studying thermal methanol. Recently, Slysh et al. (1995, 1996) made a large survey of Galactic star-forming regions in the $J_0 - J_{-1}E$ series of lines near 157 GHz and in the $6_{-1} - 5_0E$ line near 133 GHz. They detected 4 masers and 73 thermal sources at 157 GHz and 6 masers and 33 thermal sources at 133 GHz. The 157 and 133 GHz lines alone proved to be insufficient to determine some parameters of interest. We therefore observed 12 sources from the lists of Slysh et al. in the $2_K - 1_K$ series near 96 GHz. These lines were detected in space by Gottlieb et al. (1979). We chose this series because the levels 1_0E, 2_0E, $1_{-1}E$, and $2_{-1}E$ are common for the $2_{-1} - 1_{-1}E$, $2_0 - 1_0E$ lines at 96 GHz and the $2_0 - 2_{-1}E$, $1_0 - 1_{-1}E$ lines at 157 GHz. This allowed us to estimate source parameters combining the 157 and 96 GHz data.

In this paper, we describe the method and present our results; comparison of our results with the data of other investigators and more detailed analysis of source structures using the available data on other molecular species will be given in subsequent papers.

Table 1. Frequencies and line strengths of the transitions observed at 96 GHz (from Lees et al., 1973)

Transition	Frequency, MHz	Line strength
$2_{-1} - 1_{-1}E$	96739.39	1.5
$2_0 - 1_0A^+$	96741.42	2.0
$2_0 - 1_0E$	96744.58	2.0
$2_1 - 1_1E$	96755.51	1.5

2. Observations

The 133 and 157 GHz observations were made with the 12-m NRAO antenna at Kitt Peak. The beamwidth was 41″ at 133 GHz and 35″ at 157 GHz. The observations at both frequencies

Send offprint requests to: A. Winnberg

were performed with the 138-173 GHz dual polarisation SIS receiver in the position switching mode. The observations at 133 GHz were made during excellent weather conditions; typical system noise temperatures were 200 to 250 K. The system noise temperature at 157 GHz varied between 250-1000 K, depending on weather and elevation. The pointing accuracy was better than 5″. The spectra were calibrated using the standard vane method. A 768-channel hybrid spectrometer was used at both frequencies, providing velocity resolution of 0.37 km s^{-1} at 157 GHz and 0.22 km s^{-1} at 133 GHz. See Slysh et al. (1995, 1996) for more information about the observations.

The 96 GHz observations were carried out in December 1994 using the 20-m millimetre-wave telescope of Onsala Space Observatory. The receiver was tuned to the rest frequency of the $2_0-1_0A^+$ transition (96.74142 GHz). The main-beam efficiency and half-power beamwidth were 0.55 and 39″, respectively. The pointing accuracy was 5″. The observations were performed in a dual-beam switching mode with a beam separation of 11′ and a switch frequency of 2 Hz. A cryogenically cooled low-noise SIS mixer was used in the receiver. The single sideband receiver noise temperature was about 150 K. The system noise temperature, corrected for atmospheric absorption, rearward spillover and radome losses, varied between 290-900 K, depending on weather conditions and source elevation. The data were calibrated using the standard chopper-wheel method. The backend was a 256-channel filter spectrometer with 250 kHz frequency resolution. The line frequencies and strengths are presented in Table 1.

3. Results

96 GHz emission was detected in all 12 observed sources. Fig. 1 shows the line spectra. The line parameters are presented in Table 2. Table 3 shows parameters of interest for the $J_0 - J_{-1}E$ and $6_{-1} - 5_0E$ lines determined by Slysh et al. (1996). Comparison of the 96 and 157 GHz line parameters showed the following. The differences between line centre velocities at 157 and 96 GHz are much smaller than the linewidths. Thus, our results agree with the suggestion that the bulk of the emission at 157 and 96 GHz arises in a common region. Linewidths at 96 GHz are typically slightly smaller than those at 157 GHz. This is probably because the optical depths of the 96 GHz lines are smaller than those of the 157 GHz lines, as shown by statistical equilibrium calculations (see below).

The bottom row in Fig. 1 shows enlarged parts of NGC 2264, W 51Met3, and ON1 spectra with superimposed curves which represent the results of Gaussian fitting. These pictures show weak wings in the spectra of NGC 2264, W 51Met3, and possibly ON1. Similar wings are probably present in the spectra of DR 21(OH), W75N, Cep A, and S140. It is reasonable to suggest that these features dominate in the $2_1 - 1_1E$ lines toward W 51Met3, W75N, and Cep A because these lines are approximately twice as broad as the other lines in the same sources. Broad wings were also detected in the $6_{-1} - 5_0E$ line by Slysh et al. (1996) toward a number of sources. We could not fit these features by Gaussians due to their weakness and their blending with much stronger components. Further observations of these interesting features which are probably connected with high-velocity motions (bipolar outflows, cometary bow shocks of HII regions), are required.

4. Data analysis

First, we derived parameters of the sources analytically making several simplifications. Second, we made statistical equilibrium calculations to improve the obtained values and estimate their accuracy. We did not analyze DR 21MetC because of poor signal-to-noise ratio of its 96 GHz spectrum.

4.1. Analytical approach

To derive parameters of the sources analytically we had to make several assumptions. We assumed that the same homogeneous sources were observed in all the lines at 96 and 157 GHz. We also assumed a two-temperature model for methanol excitation (see for example Menten et al., 1986). This implies that the excitation temperatures of the transitions within the same K-ladders (in particular, $2_K - 1_K$) can be fitted by a single rotational temperature $T_{\rm rot}$, and that the $J_K - J_{K-1}E$ transitions (in particular, $J_0 - J_{-1}E$) have the same excitation temperature $T_{\rm KK'}$. The latter assumption is roughly in agreement with the results of statistical equilibrium calculations in the wide range of temperatures and densities that is typical for Galactic star-forming regions for levels with $J \leq 6$ and $0 \leq K \leq 2$. Note that in the case of two-temperature excitation, $T_{\rm rot}$, defined above, may be very different from the rotational temperature obtained using standard rotational diagram technique. We neglected frequency differences between the lines in the same series both for 96 and 157 GHz.

The method used in our study has considerable advantages in comparison with the widely used rotational diagram technique. First, the model with two excitation temperatures is in good agreement with the results of statistical equilibrium calculations for dense gas, and in any case better represents the real excitation temperatures of different transitions than a model with a single rotational temperature. Second, this method allowed us not to use the groundless assumption that all the lines in consideration are optically thin.

First, we determined $T_{\rm rot}$ and the optical depths of the $J_0 - J_{-1}E$ lines at 157 GHz. We did this in a way similar to that used by Menten et al. (1988b) to analyze the $J_2 - J_1E$ lines in Orion.

The optical depth in the line centre is

$$\tau = \frac{16\pi^3}{3h}\left(\frac{\ln 2}{\pi}\right)^{1/2}\mu^2 S\frac{N_l}{g_l}\left[1-\exp\left(-\frac{h\nu}{kT_{\rm KK'}}\right)\right]\frac{1}{\Delta\nu} \quad (1)$$

where μ is the dipole moment, which is equal to 1.412 Debye for b-type ($|\Delta K| = 1$) methanol transitions, and S and $T_{\rm KK'}$ are the line strength and excitation temperature, respectively. N_l/g_l is the molecular column density in the lower level divided by the statistical weight of the level; $\Delta\nu$ is the full width at half maximum of the line in hertz. Using (1) together with the

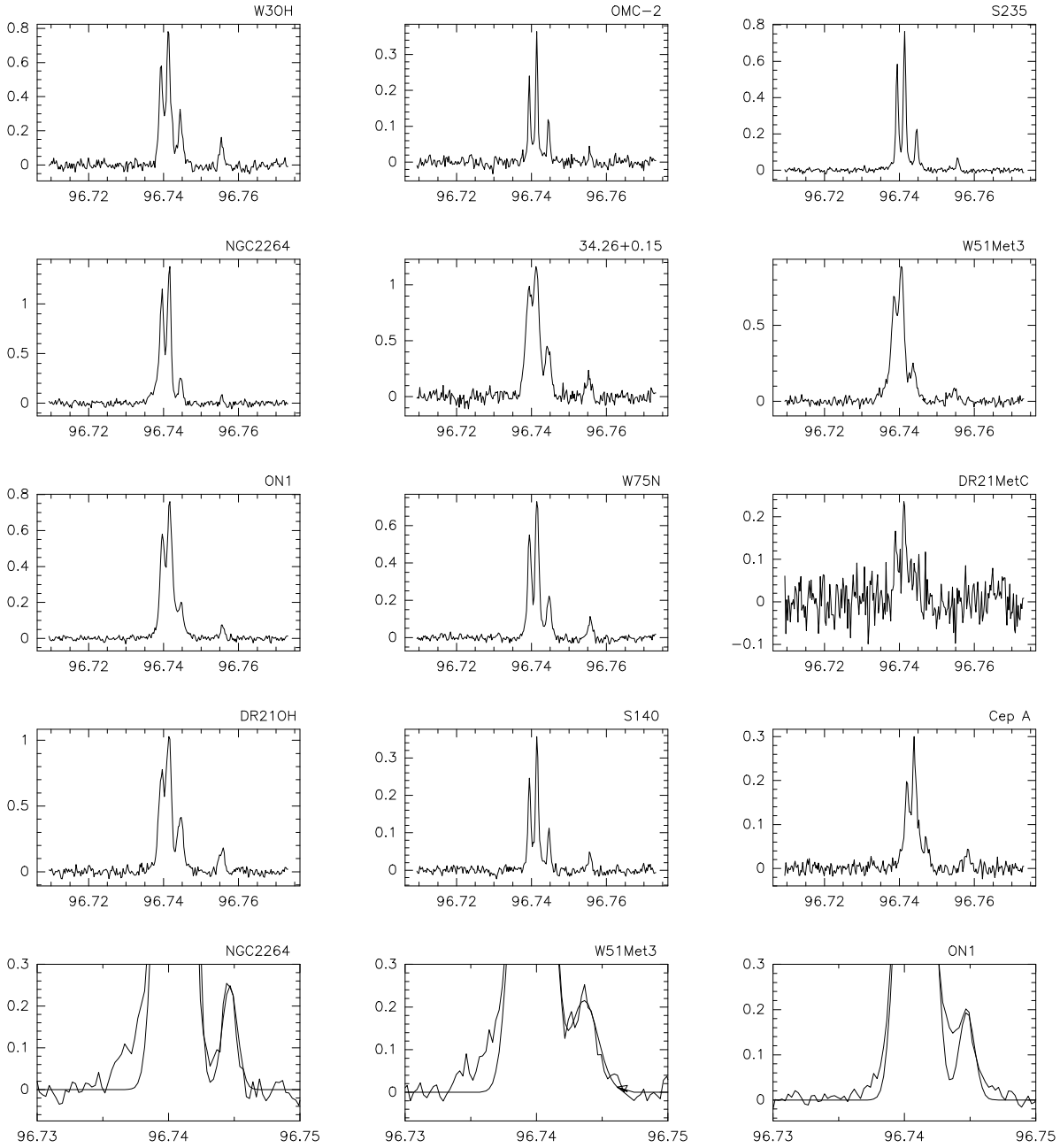

Fig. 1. Spectra of the sources observed at 96 GHz. The y-axis scale is antenna temperature in units of K and the x-axis scale is frequency in units of GHz. The bottom row shows enlarged parts of the NGC 2264, W 51Met3, and ON1 spectra with the superimposed sums of Gaussians from Table 3 to demonstrate the presence of broad wings in the NGC 2264, W 51Met3, and possibly ON1 spectra.

Boltzmann formula (2) for the levels in the backbone ladder $J_{-1}E$ and $J'_{-1}E$

$$\frac{N_J}{g_J} = \frac{N_{J'}}{g_{J'}} \exp\left(-\frac{\Delta E_{JJ'}}{kT_{\rm rot}}\right) \quad (2)$$

where $\Delta E_{JJ'}$ is the energy difference between the lower levels of the 157 GHz transitions under consideration, $J_{-1}E$ and $J'_{-1}E$, one can easily show that the optical depth τ_J of any 157 GHz line can be expressed through the optical depth τ_4 of the $4_0 - 4_{-1}E$ line:

$$\tau_J = \tau_4 \frac{S_J}{S_4} \exp\left(-\frac{\Delta E_{J4}}{kT_{\rm rot}}\right) \quad (3)$$

Combining (1)-(3) with the radiation transfer equation

$$\Delta T_{\rm R} = \frac{c^2}{2k\nu^2} [{\rm B}(\nu, T_{\rm KK'}) - {\rm B}(\nu, 2.7K)] [1 - \exp(-\tau_J)] \quad (4)$$

Table 2. Gaussian parameters of the lines detected at 96 GHz with their 1σ errors. The order of the lines: $2_{-1} - 1_{-1}E$ (upper), $2_0 - 1_0A^+$, $2_0 - 1_0E$, and $2_1 - 1_1$ (lower)

Source	RA (1950)	DEC (1950)	$V_{\rm lsr}$, km s^{-1}	ΔV, km s^{-1}	T_A^*, K
W3(OH)	02 23 17.3	+61 38 58	−46.71(0.04)	3.82(0.10)	0.57(0.01)
			−46.65(0.03)	4.45(0.09)	0.74(0.01)
			−46.70(0.09)	5.03(0.22)	0.27(0.01)
			−46.74(0.14)	4.12(0.34)	0.15(0.01)
OMC-2	05 32 59.8	−05 11 29	+10.88(0.07)	2.08(0.16)	0.22(0.01)
			+11.09(0.04)	2.11(0.09)	0.38(0.01)
			+11.25(0.08)	1.53(0.21)	0.15(0.02)
			+10.54(0.37)	1.97(0.86)	0.04(0.02)
S235	05 37 31.8	+35 40 18	−17.39(0.01)	2.34(0.03)	0.52(0.01)
			−17.27(0.01)	2.45(0.03)	0.69(0.01)
			−17.47(0.04)	2.25(0.09)	0.20(0.01)
			−17.60(0.11)	2.35(0.27)	0.06(0.01)
NGC 2264	06 38 24.9	+09 32 28	+7.12(0.04)	3.80(0.09)	0.87(0.02)
			+7.37(0.03)	3.28(0.06)	1.22(0.02)
			+7.40(0.13)	3.07(0.30)	0.22(0.02)
			+7.52(0.24)	2.44(0.57)	0.11(0.02)
34.26+0.15	18 50 46.1	+01 11 12	+57.91(0.18)	6.54(0.34)	0.91(0.02)
			+57.71(0.13)	5.30(0.25)	1.07(0.03)
			+58.33(0.14)	5.80(0.35)	0.42(0.02)
			+58.39(0.28)	5.39(0.67)	0.19(0.02)
W 51Met3	19 21 27.5	+14 23 52	+54.04(0.07)	4.68(0.17)	0.50(0.01)
			+54.34(0.05)	4.52(0.12)	0.71(0.01)
			+54.11(0.17)	4.28(0.40)	0.14(0.01)
			+53.39(0.37)	9.38(0.94)	0.09(0.01)
ON1	20 08 09.9	+31 22 42	+10.87(0.03)	4.70(0.08)	0.55(0.02)
			+11.04(0.02)	4.72(0.08)	0.72(0.02)
			+11.45(0.15)	4.30(0.36)	0.19(0.02)
			+11.04(0.05)	3.64(0.32)	0.07(0.02)
W75N	20 36 50.4	+42 27 23	+8.86(0.06)	3.14(0.13)	0.40(0.02)
			+8.86(0.04)	3.14(0.09)	0.59(0.02)
			+8.36(0.14)	3.09(0.36)	0.17(0.02)
			+7.18(0.52)	9.93(1.29)	0.08(0.01)
DR 21MetC	20 37 12.6	+42 08 46	−2.47(0.34)	3.02(0.81)	0.12(0.02)
			−2.62(0.21)	3.64(0.50)	0.21(0.02)
DR 21(OH)	20 37 13.8	+42 12 13	−3.44(0.07)	5.30(0.15)	0.62(0.01)
			−3.21(0.04)	4.39(0.09)	0.91(0.01)
			−3.04(0.07)	4.89(0.17)	0.33(0.01)
			−3.32(0.15)	5.41(0.36)	0.17(0.01)
S140	22 17 41.2	+63 03 43	−7.39(0.03)	3.14(0.08)	0.23(0.03)
			−7.31(0.03)	3.09(0.06)	0.34(0.03)
			−7.46(0.07)	2.88(0.17)	0.11(0.03)
			−7.40(0.16)	3.24(0.39)	0.05(0.03)
Cep A	22 54 19.2	+61 45 47	−10.79(0.07)	2.30(0.17)	0.10(0.01)
			−10.73(0.04)	2.78(0.11)	0.17(0.01)
			−10.63(0.14)	1.72(0.34)	0.04(0.01)
			−11.04(1.61)	5.39(3.80)	0.04(0.02)

where B is the Planck function, one can show that the ratio of the observed brightness temperature of any 157 GHz line and the $4_0 - 4_{-1}E$ line, $\Delta T_{\rm R}(J)/\Delta T_{\rm R}(4)$, can be expressed by the equation:

$$\frac{\Delta T_{\rm R}(J)}{\Delta T_{\rm R}(4)} = \frac{1 - \exp[-\tau_4\ S_J/S_4\ \exp(-\Delta E_{J4}/kT_{\rm rot})]}{1 - \exp(-\tau_4)} \qquad (5)$$

which shows that in the two-temperature model these ratios depend on two unknown parameters, $T_{\rm rot}$ and τ_4. We obtained a set of $\Delta T_{\rm R}(J)/\Delta T_{\rm R}(4)$ values using data from Table 3 and derived $T_{\rm rot}$ and τ_4 from (5) by a least-squares method. The results are presented in Table 4.

At a second step, we determined $T_{\rm KK'}$, the excitation temperature of the $J_K - J_{K-1}E$ transitions. For this purpose, we determined the ratios of populations of the levels 1_0E and $1_{-1}E$,

Table 3. Gaussian parameters of thermal lines detected at 157 and 133 GHz. The data are taken from Slysh et al. (1996). Widths and radial velocities of the $4_0 - 4_{-1}E$ line are presented.

Source	T_R^*, K						V_{lsr}	ΔV
	$1_0 - 1_{-1}E$	$2_0 - 2_{-1}E$	$3_0 - 3_{-1}E$	$4_0 - 4_{-1}E$	$5_0 - 5_{-1}E$	$6_{-1} - 5_0E$	km s^{-1}	km s^{-1}
W3(OH)[a,b]	0.58(0.01)	0.73(0.01)	0.66(0.01)	0.73(0.01)	0.69(0.01)	0.46(0.01)	−46.45(0.28)	5.52(0.66)
OMC-2[c]	0.33(0.02)	0.36(0.02)	0.34(0.02)	0.27(0.01)	0.20(0.01)	0.21(0.02)	11.45(0.06)	2.85(0.16)
S235	0.59(0.03)	0.62(0.02)	0.60(0.03)	0.44(0.02)	0.33(0.02)	0.66(0.01)	−17.01(0.07)	2.41(0.15)
NGC 2264[c]	0.58(0.03)	0.50(0.02)	0.35(0.03)	0.28(0.02)	0.20(0.02)	0.66(0.01)	7.99(0.09)	3.08(0.21)
34.26+0.15	0.97(0.02)	1.11(0.02)	0.95(0.03)	0.92(0.01)	0.78(0.01)	1.65(0.01)	58.16(0.04)	6.25(0.09)
W 51Met3[d]	0.50(0.02)	0.39(0.01)	0.30(0.03)	0.23(0.01)	0.17(0.01)		54.98(0.18)	6.95(0.44)
ON1	0.43(0.01)	0.36(0.01)	0.26(0.01)	0.22(0.01)	0.14(0.01)	0.36(0.01)	12.16(0.08)	4.49(0.19)
W75N	0.48(0.01)	0.45(0.01)	0.34(0.01)	0.31(0.01)	0.25(0.01)	0.63(0.01)	9.38(0.07)	4.24(0.18)
DR 21(OH)[c]	0.76(0.01)	0.86(0.01)	0.67(0.02)	0.69(0.01)	0.58(0.01)	1.20(0.02)	−2.74(0.03)	5.54(0.08)
S140	0.32(0.01)	0.33(0.01)	0.31(0.01)	0.29(0.01)	0.19(0.01)	0.45(0.01)	−6.81(0.06)	2.46(0.14)
Cep A[b]	0.18(0.01)	0.13(0.01)	0.11(0.01)	0.11(0.01)	0.08(0.01)	0.18(0.08)	−10.55(0.39)	5.13(0.92)

[a] J = 7 and 8 lines at 157 GHz were also used. Their corrected brightness temperatures T_R^* are 0.53(0.01) and 0.50(0.01) K, respectively
[b] Narrow maser features are present at 157 GHz
[c] Narrow maser features are present at 133 GHz
[d] Not observed at 133 GHz

using our data on the $2_0 - 1_0E$ and $2_{-1} - 1_{-1}E$ lines. These ratios are connected with $T_{KK'}$ via the expression

$$T_{KK'} = \frac{h\nu}{k \ln\left[(g_u N_l)/(g_l N_u)\right]} \quad (6)$$

where N_u/g_u and N_l/g_l are methanol column densities in the upper and lower levels, which are 1_0E and $1_{-1}E$ in our case, divided by statistical weights of the levels. Under our basic assumptions, the excitation temperatures of both 96 GHz lines in consideration are equal to T_{rot}. Taking into account that the intensities of the 96 GHz lines are typically quite different, it is reasonable to suggest that the lines are optically thin. Statistical equilibrium calculations confirm this suggestion (see next section). In this case one can obtain the following expression for the ratio of the 1_0E and $1_{-1}E$ level populations using (1) and (4) together with our basic assumptions

$$\frac{N_0/g_0}{N_{-1}/g_{-1}} = \frac{\Delta T_R(0)}{\Delta T_R(-1)} \frac{S_{-1}}{S_0} \quad (7)$$

Using (6) and (7) we can obtain $T_{KK'}$. For the sources in consideration, $T_{KK'}$ proved to be of the order of 6-10 K, i.e. much less than the kinetic temperatures of the same sources.

Note that in the analysis above, only relative line intensities were used. Thus, these results are free from calibration errors.

Knowledge of T_{rot}, $T_{KK'}$, T_{kin}, and the optical depths of the 157 GHz lines allowed us to obtain some other source parameters. We used $T_{KK'}$ and τ_4 to estimate the real, not beam-averaged, Raleigh-Jeans brightness temperature of the $4_0 - 4_{-1}E$ line $\Delta T_R(4)$. This can be obtained using the radiation transfer equation (4). Knowledge of $\Delta T_R(4)$ allowed us to obtain beam-filling factors, equal to $T_{MB}(4)/\Delta T_R(4)$, where $T_{MB}(4)$ are the $4_0 - 4_{-1}E$ main-beam brightness temperatures. Assuming the source brightness temperature distribution to be Gaussian, we can estimate the source half-power widths θ_S and the source linear sizes D, if the distances are known.

Another parameter of interest is the methanol column density. We estimated methanol column densities in the following way. First, we calculated real (not beam-averaged) methanol column densities for the $4_{-1}E$ level, N_4/g_4, using (1). Knowledge of T_{rot} and $T_{KK'}$ allowed us to obtain, within the frame of the two-temperature model, the populations of all the rotational levels, and thus to obtain E-methanol column densities. We multiplied the result by 2 to take into account A-methanol (we made the usual assumption that the A and E methanol abundances are equal). Then we estimated the methanol number densities n_{CH3OH}, by dividing N_{CH3OH} by D.

Our next step was to estimate very roughly the hydrogen number densities. We used the two-level approximation, i.e., we chose a transition with known excitation temperature, determined collisional constants, which depend on temperature and density (see formula 10), from the solution of the corresponding statistical equilibrium equation, and then calculated the density.

The excitation temperature of a line depends both on direct collisional and radiative transitions between upper and lower levels and transitions through intermediate levels. The former are taken into account by the two-level approximation, while the latter require computer modelling. To obtain a density close to the real one, we should choose a line with maximum weight of direct transitions. We believe that the best transitions for our purpose are the $J_0 - (J-1)_{-1}E$ transitions. Their Einstein coefficients of radiation decay are largest among all rotational transitions for which we can determine excitation temperature, and direct transitions between upper and lower levels determine their relative population to a large degree (see Pelling, 1975). We chose the $4_0 - 3_{-1}E$ line at 351 GHz and had to take into ac-

Table 4. Parameters of the sources obtained analytically. Columns: 1 – source name; 2 – optical depth of the $4_0 - 4_{-1}E$ line; 3 – kinetic temperature; 4 – methanol column density; 5 – calculated brightness temperature of the $4_0 - 4_{-1}E$ line; 6 – adopted distance to the source; 7 – calculated source linear size; 8 – hydrogen number density; 9 – methanol abundance (assuming equal abundances of A and E methanol)

Source	τ_4	$T_{\rm rot}$ (K)	$N_{\rm CH3OH}$ ($\rm cm^{-2}$)	$T_{\rm br}$ (K)	d (pc)	D (cm)	$n_{\rm H2}$ ($\rm cm^{-3}$)	$X_{\rm CH3OH}$
W3(OH)	2.3	37	$6.7\ 10^{15}$	3.3	2000	$8.0\ 10^{17}$	$4.7\ 10^{5}$	$1.8\ 10^{-8}$
OMC-2	0.9	15	$2.4\ 10^{15}$	4.8	500	$8.6\ 10^{16}$	$5.0\ 10^{6}$	$5.6\ 10^{-9}$
S235	0.8	13	$1.0\ 10^{15}$	1.5	2000	$1.0\ 10^{18}$	$9.9\ 10^{5}$	$1.0\ 10^{-9}$
NGC 2264	0.5	10	$7.4\ 10^{14}$	0.5	800	$1.0\ 10^{18}$	$5.3\ 10^{5}$	$1.4\ 10^{-9}$
34.26+0.15	1.7	17	$5.8\ 10^{15}$	3.0	4000	$2.1\ 10^{18}$	$1.2\ 10^{6}$	$2.3\ 10^{-9}$
W 51Met3	0.5	10	$2.1\ 10^{15}$	0.6	8000	$4.7\ 10^{18}$	$6.8\ 10^{5}$	$0.7\ 10^{-9}$
ON1	0.7	10	$1.7\ 10^{15}$	0.9	1400	$6.4\ 10^{17}$	$8.2\ 10^{5}$	$3.3\ 10^{-9}$
W75N	0.9	12	$2.3\ 10^{15}$	1.8	3000	$1.0\ 10^{18}$	$1.4\ 10^{6}$	$1.6\ 10^{-9}$
DR 21(OH)	1.9	16	$6.6\ 10^{15}$	3.8	3000	$1.1\ 10^{18}$	$1.8\ 10^{6}$	$3.4\ 10^{-9}$
S140	2.1	12	$4.4\ 10^{15}$	4.6	900	$1.6\ 10^{17}$	$3.4\ 10^{6}$	$7.9\ 10^{-9}$
Cep A	1.6	14	$3.5\ 10^{15}$	2.2	700	$1.2\ 10^{17}$	$9.9\ 10^{5}$	$2.9\ 10^{-8}$

count its optical depth; we used the following procedure. First, we calculated the $4_0 - 3_{-1}E$ line excitation temperature $T''_{\rm KK'}$ using the ratio of populations of the 4_0E and $3_{-1}E$ levels, which were obtained at the previous step. Then we calculated the parameter ϵ, the probability per scattering that a photon is lost by collisional de-excitation. This can be obtained from $\rm B(\nu'', T''_{KK'})$ using formulae presented by Hummer and Rybicki (1971). For our purpose, we arbitrarily chose the relation between ϵ and $\rm B(\nu'', T''_{KK'})$ for the outer layers of an optically thick cloud

$$\rm B(\nu'', T''_{KK'}) = \sqrt{\epsilon} B(\nu'', T_{kin}) \quad (8)$$

Knowledge of ϵ allows us to calculate the rate of collisional de-excitation C_{43} of the $4_0 - 3_{-1}E$ transition using the solution of the statistical equilibrium equation in the form

$$\epsilon = \frac{C_{\rm ul}}{C_{\rm ul} + A_{\rm ul}/[1 - \exp(-h\nu/kT_{\rm kin})]} \quad (9)$$

where $A_{\rm ul}$ is the Einstein coefficient for radiative decay from level u to level l, 4_0E, and $3_{-1}E$, respectively (Hummer and Rybicki, 1971). $C_{\rm ul}$ is connected to density via the expression for collisional constants

$$C_{\rm ul} = 1.56\ 10^{-12}\ \sqrt{T_{\rm kin}}\ n_{\rm H2} \quad (10)$$

which is in agreement with the experimental results of Lees and Haque (1974); the same collisional constant was used for this transition in the statistical equilibrium calculations (see next section).

Note, however, that although the $J_0 - (J-1)_{-1}E$ transitions are the best ones determining density using the two-level approximation, even for them it is not clear if we can neglect transitions through intermediate levels. The validity of the two-level aproximation does not follow from our basic assumptions. Only satisfactory agreement between the densities obtained as described above and those obtained by statistical equilibrium calculations (see next section) shows the validity of this approach for dense, warm gas.

Knowing the methanol and hydrogen densities, we can determine the methanol abundance $X_{\rm CH3OH}$, dividing $n_{\rm CH3OH}$ by $n_{\rm H2}$. The densities and abundances obtained are presented in Table 4.

4.2. Statistical equilibrium calculations

Statistical equilibrium (SE) calculations are necessary to check and improve the results obtained in the previous section. The approach used in this paper is that of Olmi et al. (1993). We used an LVG code kindly made available by C. M. Walmsley. The free parameters of the model are the kinetic temperature $T_{\rm kin}$, the molecular hydrogen number density $n_{\rm H2}$, and the methanol E density $n_{\rm CH3OH-E}$. Velocity gradients were chosen such that the methanol E column density divided by the linewidth for the $n_{\rm H2} - T_{\rm kin}$ plane (see below) for each source was equal to the same parameter obtained analytically. We neglected any external radiation, except the microwave background, to make the problem tractable. Some arguments showing the absence of a strong radiation field will be given elsewhere.

To obtain SE parameters, one should make statistical equilibrium calculations for a number of parameter sets and choose sets which are in agreement with the observational data. The agreement between our observations and the SE models can be evaluated by comparing the 96 and 157 GHz line intensity ratios of a model with the corresponding observed ratios. For the 96 GHz series we used the ratios $R_{\rm i} = T_{\rm MB}(2_K - 1_K)/T_{\rm MB}(2_{-1} - 1_{-1})$ of E-methanol lines ($K \neq -1$) and for the 157 GHz series we used $R_{\rm i} = T_{\rm MB}(J_0 - J_{-1}E)/T_{\rm MB}(4_0 - 4_{-1}E)$, ($J \neq 4$). The $2_1 - 1_1E$ lines in W 51Met3, W75N, and Cep A are much broader than the other 96 GHz lines. It appears that broad components dominate in these lines, and the ratios $T_{\rm MB}(2_1 - 1_1)/T_{\rm MB}(2_0 - 1_0)$ for narrow components cannot be derived from our data. Therefore, we excluded the $2_1 - 1_1E$ lines from further analysis in these sources.

Following Olmi et al. (1993), we defined χ^2 to be

$$\chi^2 = \sum_i \left(\frac{R_{\rm i}^{\rm obs} - R_{\rm i}^{\rm mod}}{\sigma_{\rm i}^{\rm obs}} \right)^2 \quad (11)$$

where $\sigma_{\rm i}^{\rm obs}$ are the rms errors of the observed ratios. The best-fit model can be found by minimizing χ^2. To find the minimum χ^2 value, we calculated χ^2 for a number of parameter sets for each source. There are 3 free parameters of the model, and to find the minimum one should vary all of them. The resulting χ^2 distribution is a three-dimensional figure in the $n_{\rm H2}, n_{\rm CH3OH-E}, T_{\rm kin}$ space. However, varying all the parameters in three-dimensional space requires an enormous amount of computing time. Therefore we made three cross-sections of the three-dimensional figure in the $n_{\rm H2} - T_{\rm kin}$, $n_{\rm CH3OH-E} - T_{\rm kin}$ and $n_{\rm H2} - n_{\rm CH3OH-E}$ planes around the "initial guesses", i.e., the values obtained analytically.

We obtained the χ^2 distribution for each source. However, the χ^2-test showed that these models should be rejected for all objects except OMC-2. One possible reason for that is wrong Gaussian fitting. Several lines both at 96 and 157 GHz are blended, especially the $J = 1 - 3$ lines at 157 GHz. We must fix some parameters to fit these lines. Therefore, the intensities may be determined incorrectly, and the actual errors may exceed the formal errors obtained by the fitting procedure. However, the most probable explanation is that the real sources are more complex than the models used in the statistical equilibrium calculations. Taking into account that the structure of the sources cannot be established without further high-resolution observations, it seems reasonable to find, using the least-squares method, sets of parameters providing the best agreement between model and observations. The scatter of the line intensity ratios depends on the unknown deviations of the real source structures from the model source structures rather than on the errors of observation. We do not know how these deviations affect line intensities, and therefore assumed that the relative deviations of line intensities are equal. We used the procedure described by Mulvey (1963) to estimate source parameters and the rms deviations of line intensities.

The best-fit model can be found by minimizing the function M', defined as

$$M' = \sum_i [(R_{\rm i}^{\rm obs} - R_{\rm i}^{\rm mod})\ w_{\rm i}]^2 \quad (12)$$

Here $w_{\rm i}$ are weight factors inversely proportional to the rms deviations $\sigma_{\rm i}$ of the ratios $R_{\rm i}^{\rm obs}$. As we assumed that the relative rms deviations of line brightness temperatures σ, equal to $\sigma(T_{\rm i})/T_{\rm i}$, are the same for all lines, $\sigma_{\rm i}^2$ is equal to $2\sigma^2/(R_{\rm i}^{\rm obs})^2$, where σ is unknown and should be evaluated. Weight factors $w_{\rm i}$ should be chosen in the form $2/R_{\rm i}^{obs}$. To find the minimum M' value, we made cross-sections in the same planes as previously to find the minimum χ^2 value for each source except OMC-2.

Knowing the minimum M' value, one can evaluate σ and find the function M, which is proportional to M' and is χ^2 distributed with $(n-p)$ degrees of freedom, using the technique described by Mulvey (1963).

Knowledge of the M distribution in the $n_{\rm H2} - T_{\rm kin}$, $n_{\rm CH3OH} - T_{\rm kin}$, and $n_{\rm H2} - n_{\rm CH3OH}$ planes allowed us to find contours enclosing "true" parameter sets. We used the χ^2 technique, described by Lampton et al. (1976).

Contours showing the M distribution (χ^2 distribution for OMC-2) are presented in Figs. 2-3. Thick lines represent contours enclosing "true" parameter sets at the 1σ confidence level. The best-fit parameters are presented in Table 5; Table 6 shows the model brightness temperatures of the $2_{-1} - 1_{-1}E$ and $4_0 - 4_{-1}E$ lines for the best-fit parameter sets. Using them, we obtained source sizes, as described in the previous section. Methanol abundance was obtained dividing the E-methanol density by the hydrogen density and multiplying by two to take into account methanol A. Figs. 2c-3c show that the increase of density together with the decrease of E-methanol density and, reversely, the increase of E-methanol density together with the decrease of density in the range of E-methanol densities $10^{-3} - 10^{-1}$ cm^{-3} do not change M'; one can understand this taking into account that the increase of both density and methanol density leads to an increase of the degree of thermalization of a source and therefore affects the ratios of the line intensities in the same manner. For E-methanol densities smaller than approximately 10^{-3} cm^{-3} all the lines in consideration become optically thin and the dependence of intensity ratios from methanol density disappears. Thus, Figs. 2c-3c show that the accuracy of density and especially methanol density determination, using the ratios of the line intensities, is low. One must know line brightness temperatures rather than their ratios to obtain these parameters. However, using Figs. 2c-3c one can determine accurately either density or E-methanol density provided that the other parameter is known. Fig. 3c shows that for ON1 the product $n_{\rm H2} \times n_{\rm CH3OH}$ is approximately constant (about $10^{2.8}$).

To reduce the suitable ranges of densities and methanol densities, we used observational data for the $6_{-1} - 5_0E$ line at 133 GHz obtained at Kitt Peak (Slysh et al., 1996). This line, unlike the 96 and 157 GHz lines, is inverted in a majority of parameter samples that minimize M'. Therefore, an increase of methanol density leads to a much larger increase of line brightness temperature at 133 GHz than at 96 and 157 GHz. We added the term $R'' = [(R_{64}^{\rm obs} - R_{64}^{\rm mod})/\sigma_{64}^{\rm obs}]^2$ to the χ^2-distributed function M. Here R_{64} is the ratio of the $6_{-1} - 5_0E$ and $4_0 - 4_{-1}E$ line intensities and $\sigma_{64}^{\rm obs}$ is the rms error of the observed ratio. Note that the $6_{-1} - 5_0E$ line was observed in another observing session at a different frequency. Under these circumstances, the accuracy of determination of R'' depends on calibration errors, pointing errors etc. Some sources were observed at low elevations; weather during the observations was sometimes bad; even small pointing errors may lead to R'' errors as large as $30 - 40\%$, because the accurate source positions are unknown and brightness peaks may be offset from the coordinates in Table 2. Therefore we adopted a 50% relative rms error of the 133 GHz line intensity, which is much larger than typical calibration errors at Kitt Peak. It is also much larger than the relative rms deviation of the line brightness temperature σ (see Table 6) for any observed source; otherwise we should use σ instead of this value.

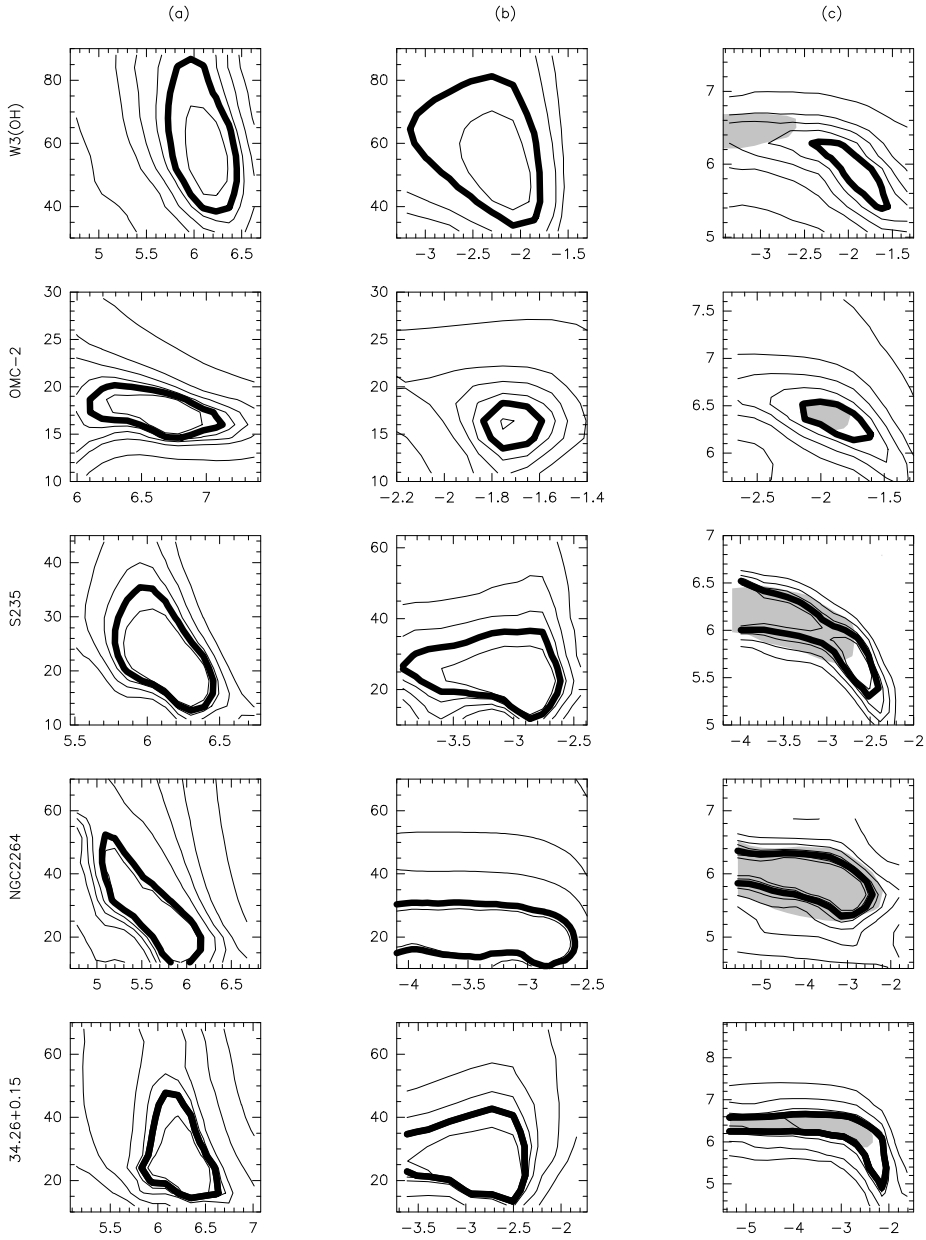

Fig. 2a–c. Contours showing the M distribution (or the χ^2 distribution for OMC-2) obtained using 96 and 157 GHz data only. Column **a** shows the distribution in the $n_{\rm H2} - T_{\rm kin}$ plane, **b** the distribution in the $n_{\rm CH3OH-\mathit{E}} - T_{\rm kin}$ plane, and **c** the distribution in the $n_{\rm H2} - n_{\rm CH3OH-\mathit{E}}$ plane. The horizontal axis in column **a** is $\log n_{\rm H2}$, cm^{-3}, the vertical axis is $T_{\rm kin}$, K. The horizontal axis in column **b** is $\log n_{\rm CH3OH}$, cm^{-3}, the vertical axis is $T_{\rm kin}$, K. The horizontal axis in column **c** is $\log n_{\rm CH3OH}$, cm^{-3} and the vertical axis is $\log n_{\rm H2}$, cm^{-3}. Thick contours correspond to threshold M (or χ^2 for OMC-2) values, i.e. they enclose "true" parameter sets with a 1σ confidence level. Other contours correspond to the levels 0.8, 1.2, 1.5, 2, and 4, multiplied by the threshold values. Shadowed regions in the $n_{\rm H2} - n_{\rm CH3OH-\mathit{E}}$ planes show areas enclosing "true" parameter sets at the 1σ confidence level, obtained using 96, 157, and 133 GHz data. The methanol densities for the $n_{\rm H2} - T_{\rm kin}$ cross-sections are 1.5E-2 for W3(OH), 1.7E-2 for OMC-2, 6.6E-4 for S235, 6.7E-4 for NGC 2264, and 1.9E-3 for 34.26+0.15. The densities for the $n_{\rm CH3OH} - T_{\rm kin}$ cross-sections are 1.6E+6 for W3(OH), 2.8E+6 for OMC-2, 1.0E+6 for S235, 0.7E+6 for NGC 2264, and 2.0E+6 for 34.26+0.15. The kinetic temperatures for the $n_{\rm CH3OH} - n_{\rm H2}$ cross-sections are 55 K for W3(OH), 20 K for OMC-2, 22 K for S235, 20 K for NGC 2264, and 25 K for 34.26+0.15.

The areas enclosing "true" parameter sets are shaded in Figs. 2c-3c. Their borders, as previously, were determined with the technique described by Lampton et al. (1976).

The ratios of the observed and model line intensities for DR 21(OH) are presented in Table 7. The table shows that the ratio $R64$ corresponding to the best-fit model is significantly smaller than observed. The same is true for the other sources, except W3(OH). To reach the observed value of $R64$, one must increase either methanol abundance or temperature relative to the best-fit model. We believe that this indicates the inhomogeneity in the sources. Probably, the significant part of the emission of the maser line $6_{-1} - 5_0E$ arises in the regions where the kinetic temperature and/or methanol abundance is enhanced relative to the regions where the bulk of thermal emission at 96 and 157 GHz appears. We suggest that the observed 133 GHz intensity is enhanced relative to the intensity of the 96 and 157 GHz sources, and so we believe that the usage of the 133 GHz data may lead to overestimation of the upper and lower limits of methanol density. Therefore we used only the upper limits of methanol densities, obtained using the 133 GHz data, and neglected the lower limits. For sources where the lower limits of methanol density cannot be derived from the 96 and 157 GHz data, we determined them from the obvious relation $T_{\rm br}^{\rm mod} \geq T_{\rm MB}$. We compared the SE and main-beam brightness temperatures for the $2_{-1} - 1_{-1}E$ line.

Liechti & Wilson (1996) mapped several methanol sources in the $4_{-1}-3_0E$ line at 36 GHz using the Effelsberg 100-m radio telescope. In particular, they mapped thermal or quasi-thermal emission in W3(OH), W75N, and DR 21OH. The source sizes in W75N and DR 21(OH) (30″ and 22″, respectively) nearly

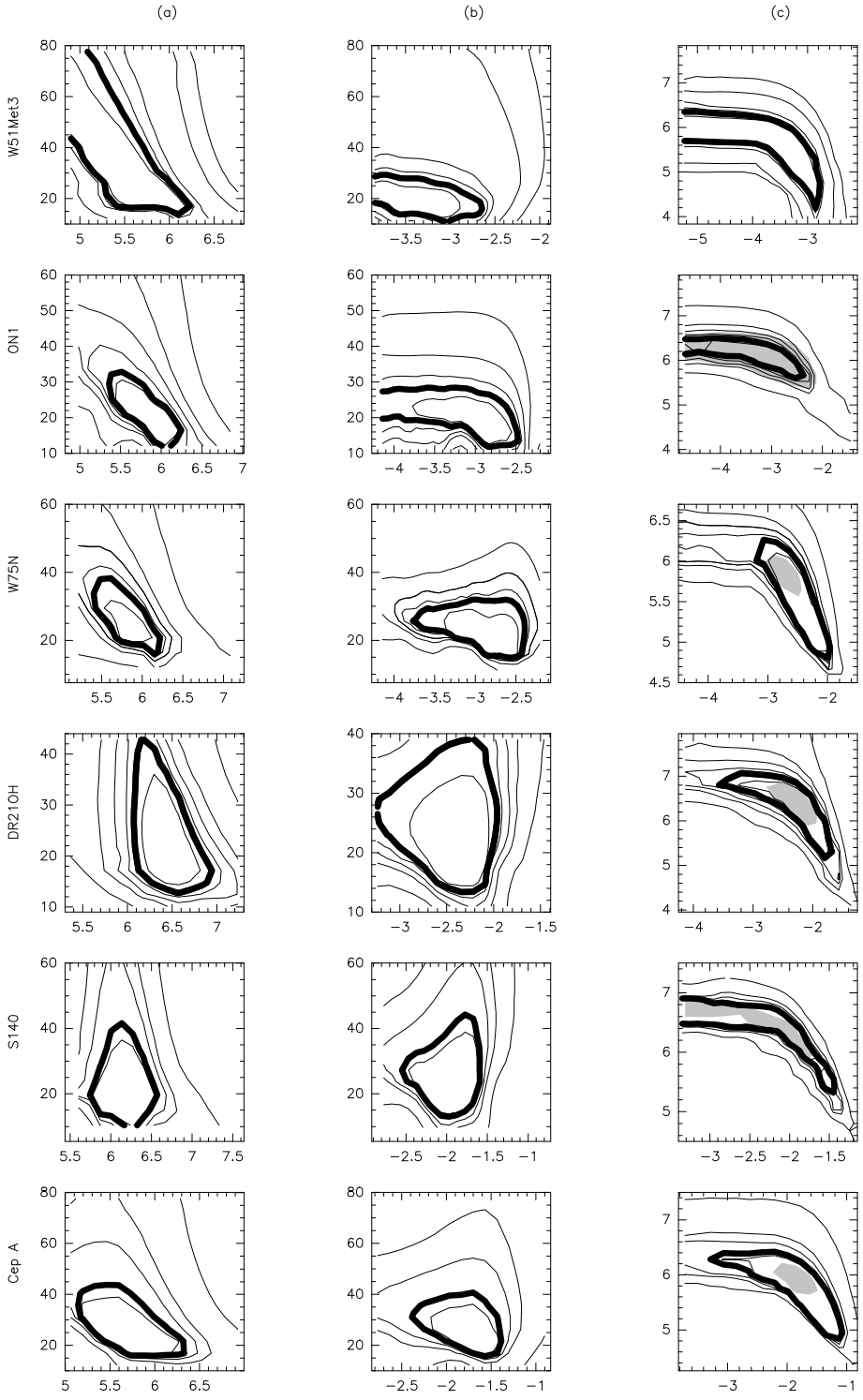

Fig. 3a–c. Same as in Fig. 2. The methanol densities for the $n_{\rm H2} - T_{\rm kin}$ cross-sections are 2.2E-4 for W 51Met3, 1.3E-3 for ON1, 1.4E-3 for W75N, 4.5E-3 for DR 21(OH), 1.5E-2 for S140, and 1.5E-2 for Cep A. The densities for the $n_{\rm CH3OH} - T_{\rm kin}$ cross-sections are 1.0E+6 for W 51Met3, 1.5E+6 for ON1, 1.9E+6 for W75N, 2.8E+6 for DR 21(OH), 2.8E+6 for S140, and 0.6E+6 for Cep A. The kinetic temperatures for the $n_{\rm CH3OH} - n_{\rm H2}$ cross-sections are 17 K for W 51Met3, 15 K for ON1, 20 K for W75N, 19 K for DR 21(OH), 18 K for S140, and 20 K for Cep A.

coincide with our best-fit values, suggesting that our best-fit estimates are close to the source parameters. The source size of 10″ in W3(OH) measured by Liechti & Wilson proved to be smaller than ours. If the source size measured by Liechti & Wilson is the same as in 96 and 157 GHz, this means that the 96 and 157 GHz line brightness temperatures are 3.2 times larger than those presented in Table 6. The best-fit density and methanol abundance will be about 3×10^5 cm^{-3} and 6×10^{-8}, respectively. We assume, however, that the source size at 36 GHz may be smaller than at 96 and 157 GHz. The $4_{-1} - 3_0 E$ line, like the $6_{-1} - 5_0 E$ line, belongs to Class I (Menten, 1991) and unlike the 96 and 157 GHz lines, it should be suppressed if the radiation is strong enough, which is probably the case in the vicinity of the compact HII-region (see Cragg et al., 1992; Kalenskii, 1995 for

Table 5. SE temperatures, densities, and A+E-methanol abundances. Best-fit values together with upper and lower limits are presented for each parameter. Only the 96 and 157 GHz data were used to derive the best-fit parameters, whereas the 96, 157, and 133 GHz data were used to derive upper and lower limits.

Source	$T_{\rm kin}$			$n_{\rm H2}$			$X_{\rm CH3OH}$		
	best	min	max	best	min	max	best	min	max
W3(OH)	50	35	85	$1.6\ 10^6$	$1.6\ 10^5$	$3.2\ 10^6$	$3.2\ 10^{-9}$	$1.6\ 10^{-9}$	$2.0\ 10^{-7}$
OMC-2	15	12	20	$4.9\ 10^6$	$7.9\ 10^5$	$1.3\ 10^7$	$7.0\ 10^{-9}$	$3.2\ 10^{-9}$	$1.0\ 10^{-8}$
S235	20	12	35	$1.0\ 10^6$	$6.3\ 10^5$	$3.2\ 10^6$	$2.4\ 10^{-9}$	$7.9\ 10^{-11}$	$5.2\ 10^{-9}$
NGC 2264	20	12	65	$5.0\ 10^5$	$1.0\ 10^5$	$2.0\ 10^6$	$2.0\ 10^{-9}$	$1.0\ 10^{-10}$	$1.0\ 10^{-8}$
34.26+0.15	22	15	45	$2.1\ 10^6$	$1.0\ 10^6$	$5.0\ 10^6$	$1.0\ 10^{-9}$	$3.2\ 10^{-11}$	$8.0\ 10^{-9}$
W 51Met3	25	10		$6.8\ 10^5$		$2.5\ 10^6$	$4.0\ 10^{-10}$	$2.5\ 10^{-11}$	
ON1	15	10	35	$8.1\ 10^5$	$2.5\ 10^5$	$2.5\ 10^6$	$1.9\ 10^{-9}$	$6.3\ 10^{-11}$	$2.0\ 10^{-8}$
W75N	25	15	35	$5.8\ 10^5$	$2.5\ 10^5$	$7.9\ 10^5$	$6.8\ 10^{-9}$	$4.0\ 10^{-10}$	$2.5\ 10^{-8}$
DR 21(OH)	18	13	40	$2.8\ 10^6$	$1.3\ 10^6$	$7.9\ 10^6$	$4.0\ 10^{-9}$	$4.0\ 10^{-11}$	$1.0\ 10^{-8}$
S140	18	15	28	$3.2\ 10^6$	$1.0\ 10^6$	$6.3\ 10^6$	$4.5\ 10^{-9}$	$7.0\ 10^{-11}$	$1.5\ 10^{-7}$
Cep A	20	15	45	$3.1\ 10^5$	$5.0\ 10^5$	$3.2\ 10^6$	$1.7\ 10^{-7}$	$3.1\ 10^{-10}$	$2.5\ 10^{-7}$

the description of methanol excitation). The linewidth presented by Liechti & Wilson (2.2 km s^{-1}) is smaller than the linewidths at both 96 and 157 GHz, in agreement with this assumption.

Comparison of the results obtained by the two methods shows that they are roughly in agreement. Tables 4 and 5 show that the source densities obtained by both methods are close to 10^6cm^{-3}, kinetic temperatures are close to 20 K for all sources except W3(OH), and methanol abundances are of the order of 10^{-9} for all sources except Cep A. For our sample of sources, the mean value of SE kinetic temperatures proved to be larger than the mean value of $T_{\rm rot}$ obtained analytically by a factor of 1.5. Densities and methanol abundances agree within a factor of 3, except for W75N and Cep A, where the SE methanol abundances are approximately 5 times higher than the same parameters obtained analytically. The 96 GHz lines proved to be optically thin for the majority of the appropriate parameter sets, including the best-fit ones; however, optical depths of the $2_{-1} - 1_{-1}E$ lines of the order of unity were obtained for models with maximum allowable methanol densities for some sources. Fig. 5 illustrates the agreement between the results. One can see that correlations between brightness temperatures, logarithms of densities, and methanol abundances indeed exist. The kinetic temperatures of all sources except W3(OH) are close to 20 K. Therefore the correlation formally exists (the correlation coefficient is 0.8), but is not reliable.

The agreement between the results obtained by the two methods makes it likely that our estimates represent parameters which are typical for the sources under consideration. However, it is noteworthy that our parameter determinations, both those obtained analytically and those obtained using statistical equilibrium calculations, strongly depend on the adopted collisional constants. We used collisional constants based on the experimental results of Lees et al. (1973) for both techniques. Their revision may require revision of the densities and probably, temperatures. The revision of densities leads to the revision of methanol abundance.

Table 6. Line brightness temperatures and source sizes that correspond to the best-fit models. The second column shows the brightness temperatures of the $4_0 - 4_{-1}E$ lines at 157 GHz, and the third column, the brightness temperatures of the $2_{-1} - 1_{-1}E$ lines at 96 GHz. Relative rms deviations of line brightness temperatures are presented in the last column

Source	$T_{\rm br}$ (K) (157 GHz)	$T_{\rm br}$ (K) (96 GHz)	θ ($''$)	D (cm)	σ (K)
W3(OH)	4.8	4.7	18	$5.3\ 10^{17}$	0.16
OMC-2	4.1	5.5	11	$8.2\ 10^{16}$	
S235	2.4	5.8	20	$6.1\ 10^{17}$	0.18
NGC 2264	1.0	3.4	156	$1.8\ 10^{18}$	0.36
34.26+0.15	4.2	5.5	24	$1.4\ 10^{18}$	0.16
W 51Met3	0.6	2.7	38	$4.5\ 10^{18}$	0.22
ON1	1.0	4.1	18	$3.7\ 10^{17}$	0.31
W75N	1.3	4.9	25	$1.1\ 10^{18}$	0.12
DR 21(OH)	5.2	8.0	17	$7.4\ 10^{17}$	0.16
S140	3.9	5.4	12	$1.6\ 10^{17}$	0.25
Cep A	3.5	12.6	8	$7.8\ 10^{16}$	0.12

In addition, the role of radiation should be studied. First, the continuum radiation, which we believe to be weak, may, however, be non-negligible. Second, radiation transfer in optically thick clouds is incorrectly described by the LVG technique if there is no velocity gradient in the real sources. This may also lead to significant errors. Thus, our estimates represent real source parameters provided that the adopted collisional constants are close to the real ones, the continuum radiation is negligible, and LVG model adequately describes the clouds.

Further observations are necessary to test our estimates. The best test is high-resolution observations of thermal methanol, suitable to test both our basic assumptions about the structure of the sources and our estimates of the source brightness temperatures and sizes. One can observe the $J_1 - J_0E$ series of lines near 165 GHz and estimate source parameters using 165 GHz

Table 7. Ratios of line intensities corresponding to the best-fit model and to models with minimum and maximum parameters in agreement with the observations for DR 21(OH). The values of the corresponding parameters are presented in Table 5. The ratios are: $R14-(1_0-1_{-1}E)/(4_0-4_{-1}E)$; $R24-(2_0-2_{-1}E)/(4_0-4_{-1}E)$; $R34-(3_0-3_{-1}E)/(4_0-4_{-1}E)$; $R54-(5_0-5_{-1}E)/(4_0-4_{-1}E)$; $R0\text{-}1-(2_0-1_0E)/(2_{-1}-1_{-1}E)$; $R1\text{-}1-(2_1-1_1E)/(2_{-1}-1_{-1}E)$; $R64-(6_{-1}-5_0E)/(4_0-4_{-1}E)$

Ratios	$R14$	$R24$	$R34$	$R54$	$R0$-1	$R1$-1	$R64$
Observed	1.10	1.24	0.97	0.84	0.53	0.27	1.72
Best-fit	1.10	1.16	1.12	0.79	0.70	0.23	0.85
Minimum temperature	1.36	1.35	1.26	0.57	0.70	0.22	0.32
Maximum temperature	0.78	0.97	1.03	0.92	0.67	0.20	1.70
Maximum density (min. methanol abund.)	1.06	1.38	1.31	0.64	0.72	0.25	0.29
Minimum density (max. methanol abund.)	0.78	1.09	1.07	0.83	0.75	0.27	4.81

line intensities instead of 157 GHz intensities. The 165 GHz lines probably are more suitable for the determination of source parameters, because they are not blended and their intensities can be obtained more accurately. In addition, one can observe $^{13}CH_3OH$ lines to test optical depths and methanol column densities and other molecules that trace high-density gas to make independent estimates of gas parameters.

5. Discussion

In this section, we briefly discuss our results; more detailed analysis and comparison of our results with data of other investigators will be given in subsequent papers.

Tables 4, 5, and 6 show that the source densities are of the order of 10^6 cm^{-3} and kinetic temperatures of the order of 20 K, with only one exception – W3(OH). The source sizes are of the order of 10^{18} cm. Similar sizes have been obtained in interferometric observations of some star-forming regions in the lines of CS and of other high-density gas tracers (Plambeck and Menten, 1990; Pratap and Menten, 1993). The uncertainties of E-methanol abundance determinations are very large. One can notice, however, that the values providing the best fit to the observational data are enclosed in the range $4\times10^{-10}-1.2\times10^{-8}$ for all sources except Cep A. Such abundances are typical for dark clouds (Friberg et al., 1988; Kalenskii and Sobolev, 1994) and are much smaller than the methanol abundance in Ori-KL and some other "hot cores"(Menten et al., 1986, 1988a) or in regions with young bipolar outflows (Bachiller et al., 1995). The methanol abundance in Cep A providing the best fit to observational data, proved to be 1.7×10^{-7}; however, the lower limit of the abundance is below 10^{-9}.

Slysh et al. (1994) detected the $1_0-0_0A^+$ methanol line toward a number of molecular clouds and determined the methanol abundance for the majority of them. Their results were revised by Kalenskii and Sobolev (1994). Our methanol abundance agrees within a factor of two with the values obtained by Kalenskii and Sobolev for common sources – NGC 2264, ON1, and DR 21(OH).

The best-fit kinetic temperatures from Table 4 are typically about 1.5 times smaller than kinetic temperatures derived from ammonia observations of the same sources (Batrla et al., 1983; Churchwell et al., 1990; Güsten & Ungerechts, 1985; Mauersberger et al., 1986; Wouterloot et al., 1988). It is possible that we simply missed good parameter samples with temperatures, close to the ammonia ones. This could be the case, because we made cross-sections around "initial guesses" instead of varying temperature, density, and methanol abundance over the whole region of their possible values. To check this possibility, we made cross-sections in the $n_{\rm H2}-n_{\rm CH3OH-E}$ planes for 34.26+0.15, DR 21(OH), and Cep A, taking kinetic temperatures equal to the ammonia ones. In all cases we obtained worse fits ($M'_{\rm min}$ for ammonia temperatures proved to be 10 - 50% larger than for methanol temperatures) and therefore our temperature estimates agree better with the 96 and 157 GHz data. We believe that this discrepancy may be due to variations of gas temperature along the lines of sight. Note that most of the upper levels of the 96 and 157 GHz lines are below 20 K, and therefore our analysis relates to very cold gas.

No correlations between source sizes and linewidths or between densities and linewidths were found. This is not surprising because large scatter is typical for these dependencies and large data sets are necessary to establish them.

Thus, our results show that massive young stars are often associated with clumps of gas with temperatures 20-50 K, densities of the order of 10^6 cm^{-3}, methanol abundance of the order of $10^{-9}-10^{-8}$, and sizes of about 0.3 pc.

6. Summary and conclusions

1. We observed 12 regions of massive star formation in the 2_K-1_K series of methanol lines near 96 GHz. Emission was detected toward all the observed sources. Radial velocities of the lines proved to be similar to the radial velocities of the methanol lines $J_0-J_{-1}E$ near 157 GHz. The linewidths at 96 GHz are slightly smaller than those at 157 GHz, suggesting that the optical depths at 96 GHz are smaller.
2. We derived a number of source parameters both analytically and using statistical equilibrium calculations. The parameters determined by the two methods are close to each other.

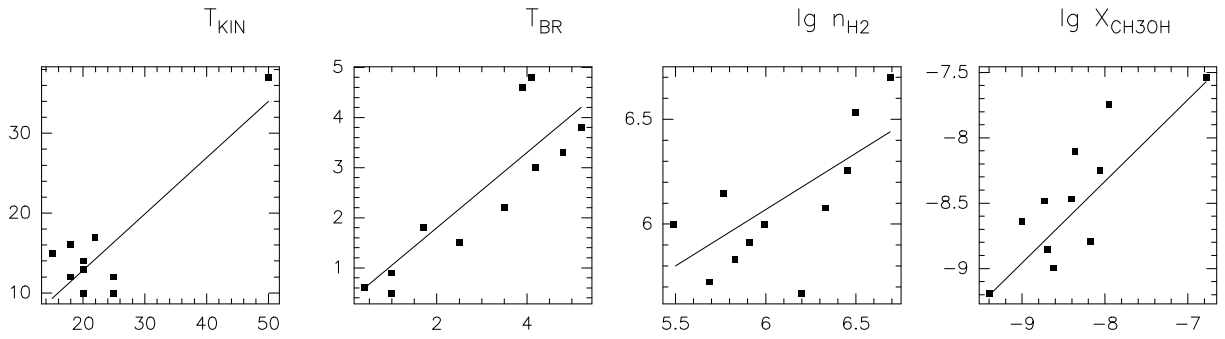

Fig. 4. Comparison of the SE and analytical source parameters. The horizontal axis represents SE parameters, the vertical axis represents parameters determined analytically. The vertical axis of the left graph represents $T_{\rm rot}$ instead of $T_{\rm kin}$. The solid lines show regressions between the two estimates. Correlation coefficients are: 0.8 for kinetic and rotational temperatures, 0.9 for brightness temperatures, 0.7 for logarithms of density, and 0.8 for logarithms of methanol abundance.

However, our estimates are based on simplified source models and at best represent some typical source parameters.

3. The source densities vary in the range $0.3 - 5 \times 10^6$ cm^{-3} and kinetic temperatures in the range 15-50 K. Source sizes are of the order of 10^{18} cm; similar sizes were obtained from the interferometric observations of some star-forming regions in the lines of CS and of other high-density gas tracers. Methanol abundance can be determined only with large errors; the values which provide the best agreement with the observational data for all sources except Cep A are enclosed in the range $4 \times 10^{-10} - 1.2 \times 10^{-9}$, typical for dark clouds rather than for "hot cores".
4. Broad components were detected in the 96 GHz spectra of several objects. These wings are probably connected with high-velocity motions in star-forming regions (bipolar outflows, cometary bow shocks of HII regions).

Acknowledgements. We are grateful to the staff of the Onsala Space Observatory for providing help during the observations. We would like to thank Drs. V. I. Slysh and I. E. Val'tts for helpful discussions, the anonymous referee for useful comments, Drs. M. Kutner and K. Mead for providing helpful information about the calibration at the 12-m Kitt-Peak antenna, Dr. D. Gabuzda for critically reading the manuscript, and V. Golubev for help during the preparation of this paper. The work was done under partial financial support of the Russian Foundation for Basic Research (grant No 95-02-05826), International Science Foundation (grants No MND000 and MND300), Royal Swedish Academy of Sciences, and European Southern Observatory. The Onsala Space Observatory is the Swedish National Facility for Radio Astronomy and is operated by Chalmers University of Technology, Göteborg, Sweden, with financial support from the Swedish Natural Science Research Council and the Swedish Board for Technical Development.

References

Ball J.A., Gottlieb C.A., Lilley, A.E., Radford, H.E. 1970, ApJ 162, L203

Bachiller R., Liechti S., Walmsley C.M., Colomer F. 1995, A&A, 295, L51

Batrla W., Wilson T.L., Bastien P., Ruf K. 1983, A&A, 128, 279

Cezaroni R., Walmsley C.M., Churchwell E. 1992, A&A, 256, 618

Churchwell E, Walmsley C.M., Cesaroni R. 1990, A&AS, 83, 119

Cragg D.M., Johns K.P., Godfrey P.D., Brown R.D., 1992, MNRAS 259, 203

Friberg P., Madden C.S., Hjalmarson Å., Irvine, W.M. 1988, A&A 195, 281

Gottlieb C.A., Ball J.A., Gottlieb E.W., Dickinson, D.F. 1979, ApJ 227, 422

Güsten R., Ungerechts H. 1985, A&A, 145, 241

Hummer D.G., Rybicki G. 1971, Ann. Rev. Astron. Astrophys. 9, 237

Kalenskii S.V. 1995, Astronomy Reports 39, 465

Kalenskii S.V., Sobolev A.M. 1994, Astronomy Letters, 20, 91

Lampton M., Margon B., Bowyer S., 1976, ApJ 208, 177

Lees R.M., Lovas F.J., Kirchoff W.H., Johnson D.R. 1973, J. Phys. Chem. Ref. Data, 2, 205

Lees R.M., Haque S.S. 1974, Canadian J. of Phys. 52, 2250

Liechti S., Wilson T.L., 1996, A&A, 314, 615

Mauersberger R., Henkel C., Wilson T.L., Walmsley C.M. 1986, A&A, 162, 199

Menten K.M., in Skylines, Proceedings of the Third Haystack Observatory Meeting, p. 119, eds. A.D. Haschick and P.T.P. Ho (Astr. Soc. Pac.)

Menten K.M., Walmsley C.M., Henkel C., Wilson T.L. 1986, A&A, 157, 318

Menten K.M., Walmsley C.M., Henkel C., Wilson T.L. 1988a, A&A, 198, 253

Menten K.M., Walmsley C.M., Henkel C., Wilson T.L. 1988b, A&A, 198, 267

Mulvey J.H., 1963, Statistical Methods in the Treatment of Experimental Data. In: Galbraith W., Williams W.S.C. (eds.) High Energy and Nuclear Physics Data Handbook. Chilton, sect. 14

Olmi L., Cesaroni R., Walmsley C.M. 1993, A&A, 276, 489

Plambeck R.L., Menten K.M. 1990, ApJ 364, 555

Pratap P., Menten K.M. 1993, Lecture Notes in Physics 412, 211

Slysh V.I., Bachiller R., Berulis I.I., Val'tts I.E., Gomez-Gonzalez J., Kalenskii S.V., Colomer F., Martin-Pintado J., Rodriguez-Franco A., 1994, Astronomy Reports 38, 29

Slysh V.I., Kalenskii S.V., Val'tts I.E. 1995, ApJ 442, 668

Slysh V.I., Kalenskii S.V., Val'tts I.E., Alakoz A.V., Golubev V.V. 1996, in preparation

Wouterloot J.G.A., Walmsley C.M., Henkel C. 1988, A&A, 203, 367

This article was processed by the author using Springer-Verlag LaTeX A&A style file *L-AA* version 3.